BULLETIN OF THE POLISH ACADEMY OF SCIENCES
TECHNICAL SCIENCES
Vol. 55, No. 2, 2007

Invited paper

Bio-inspired mechanics of bottom-up designed hierarchical materials: robust and releasable adhesion systems of gecko

H. YAO[1] and H. GAO[2*]

[1]Max Planck Institute for Metals Research, Heisenbergstr. 3, 70569 Stuttgart, Germany
[2]Division of Engineering, Brown University, Providence, RI 02912, USA

Abstract. To explore the basic principles of hierarchical materials designed from nanoscale and up, we have been studying the mechanics of robust and releasable adhesion nanostructures of gecko [1]. On the question of robust adhesion, we have introduced a fractal-like hierarchical hair model to show that structural hierarchy allows the work of adhesion to be exponentially enhanced as the level of structural hierarchy is increased. We show that the nanometer length scale plays an essential role in the bottom-up design and, baring fracture of hairs themselves, a hierarchical hair system can be designed from nanoscale and up to achieve flaw tolerant adhesion at any length scales. For releasable adhesion, we show that elastic anisotropy leads to orientation-dependent adhesion strength. Finite element calculations revealed that a strongly anisotropic attachment pad in contact with a rigid substrate exhibits essentially two levels of adhesion strength depending on the direction of pulling.

Key words: nanotechnology, nanoengineering, bio-inspired mechanics, bottom-up design, hierarchical materials, adhesion, biological material, contact mechanics, anisotropic materials.

1. Introduction

Among hundreds of animal species for which adhesion plays an important role for survival, gecko stands out in terms of body weight and its extraordinary ability to manoeuvre on vertical walls and ceilings [2]. Recent experimental measurements [3–6] have provided evidence that the adhesion ability of gecko is primarily due to the van der Waals interaction [7] between a contacting surface and gecko's hairy feet which contain hundreds of thousands of keratinous hairs called setae (Figs. 1a,b); each seta is about 110 μm long and branches near its tip region into hundreds of thinner fibrils called spatulae arranged in a fractal-like hierarchical pattern (Fig. 1c). While it is remarkable that gecko can make use of the relatively weak van der Waals interactions to manoeuvre on unpredictable rough surfaces under harsh environmental conditions, it may be even more impressive that such robust adhesion appears to be easily releasable during animal locomotion. What are the mechanics principles behind such robust and releasable adhesion in biology?

Contact mechanics theories have been used to understand adhesion mechanisms in both engineering and biology. The classical Hertz theory [8] assumes no adhesive interactions between contacting objects. Johnson et al. [9] extended the Hertz theory to contact between adhesive elastic spheres and developed the JKR (Johnson-Kendall-Roberts) model in which the contact area is determined via a balance between elastic and surface energies similar to Griffith's criterion [10] for crack growth in an elastic solid. The JKR theory introduces into the Hertz solution an additional crack-like singular term which satisfies the Griffith condition near the contact edge. While the JKR theory is quite appropriate for modelling contact between large and soft materials, the assumption of a crack-like singular field becomes increasingly inaccurate for small and stiff materials, in which case different assumptions on the elastic deformation of contacting objects have led to the models of DMT (Derjaguin-Muller-Toporov) [11] and Bradley [12]. Maugis [13] generalized the Dugdale model of a crack in a plastic sheet [14] to adhesive contact and developed a more general model (Maugis-Dugdale model) that includes the JKR and DMT models as two limiting cases. More recent studies have further extended these theories to viscoelastic materials [15,16], coupled normal and shear loads [17] and biological attachments [4,6,18–21].

For contact between single asperities, one can define adhesion strength as the tensile force per unit contact area at pull-off, which can be maximized at the theoretical adhesion strength via size reduction [22-25]. In this respect, it is interesting to note that the existing contact mechanics theories, including JKR, DMT and Maugis-Dugdale models, all predicted infinite adhesion strength as the size of contacting objects is reduced to zero. This behaviour is unphysical because the adhesion strength can not exceed the theoretical strength of adhesive interaction. The fact that this behaviour also occurs in the Maugis-Dugdale model is especially peculiar since the original Dugdale model correctly predicted that the fracture strength is bounded by the yield strength of the material. Gao et al. [23] studied this problem and found that the root of this

*e-mail: huajian_gao@brown.edu

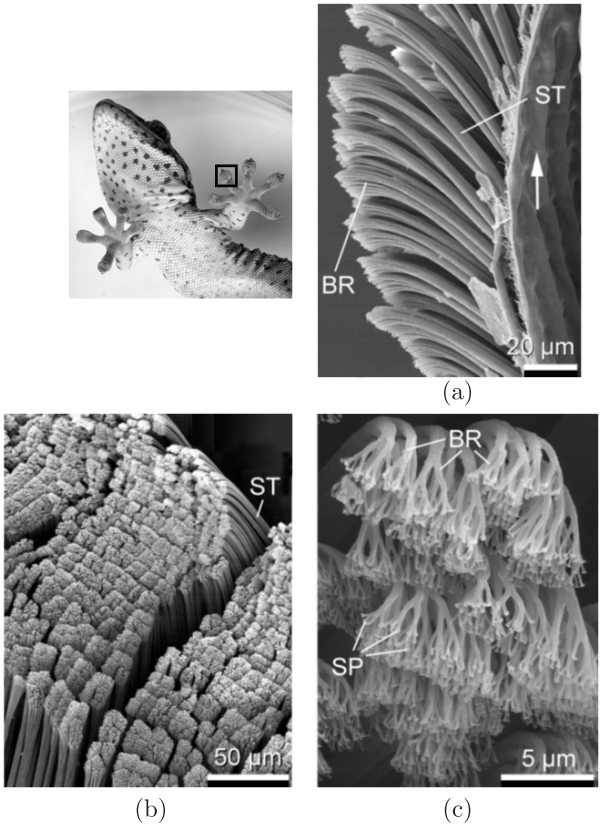

Fig. 1. The hierarchical adhesion structures of Gekko gecko. A toe of gecko contains hundreds of thousands of setae and each seta branches near its tip region into hundreds of spatulae. (a) and (b): scanning electron micrographs of setae at different magnifications. (c): spatulae, the finest terminal branches of seta. ST: seta; SP: spatula; BR: branch. (Adapted afer Ref. 24)

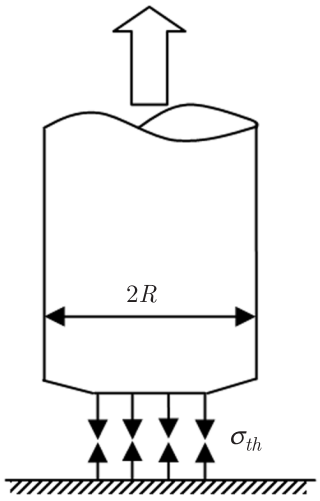

Fig. 2. Flaw tolerance state of adhesion over a partially cracked region

unphysical behaviour of the classical contact models can be traced back to the original Hertz approximation of contact surface profiles as parabolas, which is strictly valid only if the size of the contact area is much smaller than the overall dimension of the contacting objects; the lack of strength saturation in these models is thus explained from the fact that the parabolic approximation fails in the limit of very small contacting bodies. As an example, Gao et al. [24] showed that, if the exact geometry of a sphere in contact with a flat surface is considered, the adhesion strength indeed saturates at the theoretical strength as the diameter of the sphere is reduced to zero. On the other hand, Gao and Yao [23] showed that the adhesion strength can in principle approach the theoretical strength for any contact size via shape optimization. In practice, interfacial crack-like flaws due to surface roughness or contaminants inevitably weaken the actual adhesion strength. Gao et al. [24] performed finite element calculations to show that the adhesion strength of a flat-ended cylindrical punch in partial contact with a rigid substrate (Fig. 2) saturates at the theoretical strength below a critical radius around 200 nm for the van der Waals interaction. Similar discussions of strength saturation for small contacting objects have been made by Persson [22] for a rigid cylindrical punch on an elastic half-space and by Glassmaker et al. [25] for an elastic cylindrical punch in perfect bonding with a rigid substrate. Gao and Yao [23] showed that the theoretical strength can be achieved by either optimizing the shape of the contact surfaces or by reducing the size of the contact area; the smaller the size, the less important the shape. A shape-insensitive optimal adhesion can be realized below a critical contact size, which can be related to the intrinsic capability of a small scale material to tolerate crack-like flaws [26–28]. Hui et al. [29] and Glassmaker et al. [25] demonstrated that fibrillar structures with slender elastic fibrils can significantly enhance the adhesion strength. Northen and Turner [30] made use of massively parallel MEMS processing technology to produce hierarchical hairy adhesive materials containing single slender pillars coated with polymer nanorods, and reported significantly improved adhesion in such multiscale systems.

In contrast to the increasing volume of research on robust adhesion, the question of how adhesion is released upon animal movement has so far received relatively little attention. Autumn et al. [3] reported experimental data that the pull-off force of an individual seta of gecko depends strongly on the pulling angle. Gao et al. [24] numerically simulated the pull-off force of a single seta and found that the asymmetrical alignment of seta allows the pull-off force to vary strongly (more than an order of magnitude) with the direction of pulling.

Previous studies have provided significant insights into various aspects of adhesion mechanisms in biology. However, a general understanding is still lacking with respect to a number of critical issues. First, robust adhesion at the level of a single hair or fibre does not automatically address the problem of robust adhesion on rough surfaces at macroscopic scales. It has been shown that size reduction can result in optimal adhesion strength at the level of a single fibre [22–25]. However, it is not clear how this size induced optimization might work at the system level of hierarchical structures. Similarly, releasable adhesion at the level of a single seta [3,24] does not provide full expla-

nations on how releasable adhesion is achieved in macroscopic contact. The present paper is aimed to discuss the basic mechanics principles which underline these issues. For robust adhesion, we show that the fractal-like spatula ultrastructure of gecko provides a systematical strategy to optimize adhesion strength at larger length scales. We show that, given sufficient hierarchical levels, a fractal hairy system can be designed using a bottom-up approach to achieve robust, flaw tolerant adhesion at any macroscopic length scales. However, consideration of crack-like flaws in the hairs themselves imposes an upper bound on the length scale for robust adhesion. For releasable adhesion, we show that macroscopic elastic anisotropy allows the adhesion strength to vary strongly with the direction of pulling, leading to an orientation-controlled switch between attachment and detachment. The bottom-up design principles of the hierarchical structures of gecko provide not only a foundation to understand more general adhesion mechanisms in biology but also suggest novel adhesive materials for engineering applications.

2. Bottom-up designed hierarchical structures for robust adhesion

2.1. Flaw tolerant adhesion of a single fibre. Adhesive contact between elastic objects usually fail by propagation of crack-like flaws initiated at poor contact regions around surface asperities, impurities, trapped contaminants, etc. As an external load is applied to pull the contacting objects apart, stress concentration is induced near the edges of contact regions around surface asperities. With increasing load, the intensity of stress concentration at the largest interfacial flaw will first reach a critical level and the contact starts to fail by crack growth and coalescence. Under this circumstance, the adhesion strength is not optimal because only a small fraction of material is highly stressed at any instant of loading. From the robustness point of view, it would be best to seek a design of material that allows the contact to fail not by crack propagation, but by uniform detachment at the theoretical strength of adhesion (e.g. see Fig. 2 for a partially cracked adhesion case), corresponding to achieving equal load sharing at the point of failure, a concept also termed as 'flaw tolerance' [24,26–28]. According to this concept, in an ideal flaw tolerant adhesion system, there should be no crack propagation and coalescence as the contact interface is pulled apart by uniform detachment.

For a single fibre on substrate, Gao and Yao [23] have investigated the condition for flaw tolerant adhesion from the point of view of variations in contact shape. It was shown that flaw tolerant adhesion can be achieved when the size of the fibre is reduced to below a critical size given by

$$R_{cr} = \frac{8}{\pi}\frac{E_f W_{ad}}{(1-\nu_f^2)\sigma_{th}^2}, \qquad (1)$$

where E_f and ν_f are Young's modulus and Poisson's ratio of the fibre; W_{ad} and σ_{th} are the work of adhesion and theoretical adhesion strength. Alternative derivations based on partial contact [24] or perfectly bonded contact [25] lead to similar, but more relaxed, conditions on the fibre size. Therefore, we shall adopt Eq. (1) as the basic flaw tolerant condition for adhesion of a single fibre. The concept of flaw tolerance has also been discussed by Gao and Chen [28] for the simple scenario of an elastic tensile strip containing an arbitrarily sized internal or edge crack.

2.2. Energy dissipation in fibrillar structures. It can be seen from Eq. (1) that R_{cr} is proportional to the work of adhesion W_{ad} which is commonly taken as the surface energy $\Delta\gamma = \gamma_f + \gamma_s - \gamma_{fs}$, where γ_f, γ_s, γ_{fs} denote the surface energies of fibre, substrate and fibre-substrate interface respectively. This interpretation, however, is appropriate only in the absence of other dissipation mechanisms. For slender elastic hairs in strong, flaw tolerant adhesion with a solid surface, additional energy dissipation terms should be taken into account.

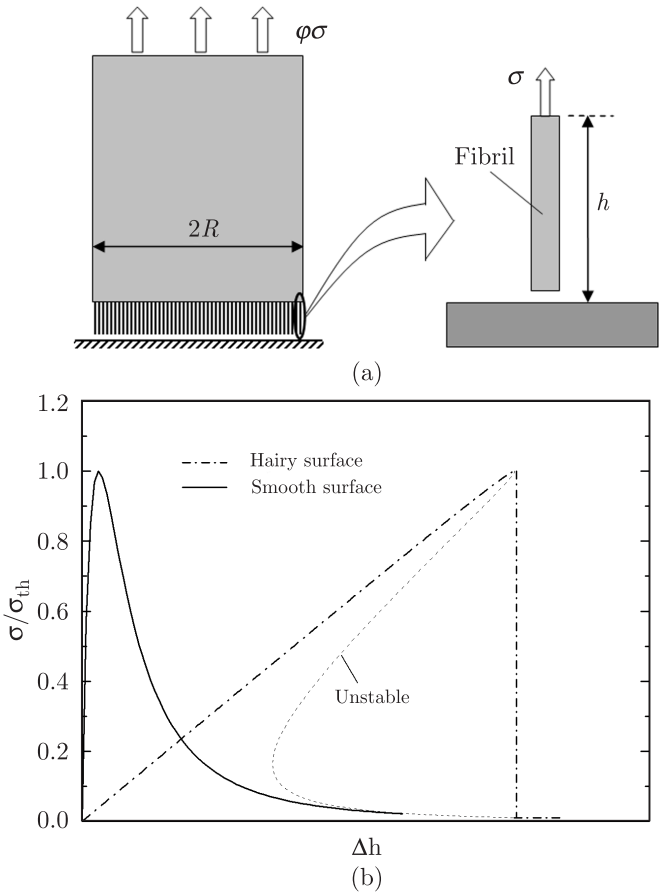

Fig. 3. Work of adhesion of a hairy surface. (a) Schematic of a hairy surface containing arrays of fibrillar protrusions contacting a substrate. (b) Effective stress-separation law for the hairy surface on substrate versus that for two smooth surfaces

To illustrate this point, let us consider the adhesion between a larger fibre with a hairy surface in contact with a substrate, as shown in Fig. 3(a). Compared to the normal case of contact with a smooth surface, the larger fibre in Fig. 3(a) contains a number of thinner fibrils on its

tip surface, resulting in a two-levelled structure: an array of smaller fibrils on the tip surface of a larger fibre. For this structure, the work of adhesion for the larger fibre is no longer equal to $\Delta\gamma$ even though the small fibrils interact with the substrate only via van der Waals forces. To estimate the work of adhesion of the large fibre, we assume that the fibrils are thin enough to meet the condition for flaw tolerant adhesion. Fig. 3(b) plots the effective stress-separation relationship for the hairy surface, assuming Lennard-Jones [31] interaction law. While the stress-separation curves for two smooth surfaces are described by the van der Waals interaction laws at the atomic scale, the separation at the level of the larger fibre is strongly influenced by the elastic properties and geometry of the fibrils. For sufficiently long fibrils, the elastic deformation of the fibrils will make significant contributions to the separation process, and adhesion failure occurs by an abrupt drop in stress near the theoretical strength of surface interaction. In this way, the strain energy stored in the fibrils is dissipated through dynamic snapping, resulting in an additional component to the work of adhesion. In other words, the thin fibrils behave effectively as cohesive bonds for the larger fibre. The work of adhesion for the large fibre should therefore include the elastic energy stored in the fibrils when they are stretched to failure, i.e.

$$W_{ad} = \left(\Delta\gamma + \sigma_{th}^2 L/2E_f\right)\varphi, \tag{2}$$

where L is the length of the fibrils and φ is the area fraction of the fibril array. The first term within the bracket represents the original van der Waals interaction energy and the second term is the elastic energy lost during dynamic snapping of the fibrils as they are detached from the substrate near the theoretical strength of van der Waals interaction. Eq. (2) also shows why it is important to optimize the strength of the lower level fibril structure via size reduction: the strength of the lower scale fibrils directly contributes to the work of adhesion of the larger scale fibre. Taking $\Delta\gamma = 0.01$ J/m^2, $\sigma_{th} = 20$ MPa, $L = 100$ μm, $E_f = 1$ GPa, $\varphi = 0.5$, the work of adhesion for the hairy tipped fibre is calculated to be $W_{ad} \approx 10$ J/m^2, a value much larger than $\Delta\gamma$. Such enhancement in work of adhesion by fibrillar structures has been reported or discussed by Jagota and Bennison [32], Persson [20], Gao et al. [27] and Tang et al. [33]. Hence, slender hairs with large aspect ratio can significantly increase the work of adhesion and contribute to the robustness of adhesion at larger scales. However, the length of the fibrils can not be too long as there is an instability leading to fibre bunching as the aspect ratio of the fibrils increases. This is discussed in the following subsection.

2.3. Anti-bunching condition in fibrillar structures. In an array of slender hairs planted on a solid surface, the van der Waals interaction between neighbouring fibres can cause them to bundle together when the aspect ratio of the fibres is large enough [20,24,34–37]. For the hairy adhesion structures, it is necessary to prevent the fibres from bunching in order to ensure the proper adhesion function. The exact form of the anti-bunching condition depends on the geometry of the fibre. For example, the anti-bunching condition for fibres of square cross section has been derived by Hui et al. [35] and Gao et al. [24]. In this paper, we focus on cylindrical fibres that have been investigated by Glassmaker et al. [37].

Consider two neighbouring identical cylindrical fibres with circular cross sections. When the separation $2w$ becomes small, the surface adhesive forces may cause them to bundle together, as shown in Fig. 4(a). The stability condition can be derived from the point of view of a maximum fibre length for spontaneous separation of two fibres sticking together [24]. In other words, given fibre separation $2w$ and radius R, there exists a critical length L_{cr} beyond which lateral bunching of neighbouring fibres becomes stable configurations. Assuming that the fibres are distributed in a regular lattice pattern, the critical length for bunching of cylindrical fibres can be expressed as [37]

$$\begin{aligned} L_{cr} &= R\alpha \left(\frac{E_f R}{\gamma_f}\right)^{1/3} \left(\sqrt{\varphi_{\max}/\varphi} - 1\right)^{1/2}, \\ \alpha &= \left[\frac{3^3\pi^4}{2^5(1-\nu_f^2)}\right]^{1/12}, \end{aligned} \tag{3}$$

where $\varphi_{\max}$ stands for the maximum value of area fraction for a given hair distribution pattern. It can be shown that $\varphi_{\max} = \pi/2\sqrt{3}$ for a triangular lattice (Fig. 4b), $\varphi_{\max} = \pi/4$ for a square lattice (Fig. 4c) and $\varphi_{\max} = \pi/3\sqrt{3}$ for a hexagonal lattice (Fig. 4d).

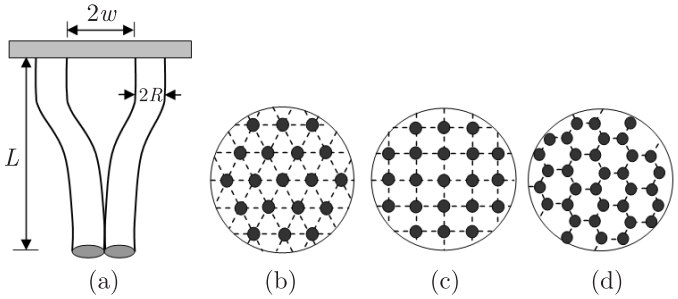

Fig. 4. Anti-bunching condition of a fibrillar structure. (a) Configuration of self-bunching in an array of fibres distributed in (b) triangular, (c) square or (d) hexagonal patterns

Equation (3) has been derived for the lateral sticking between two neighbouring fibrils. Similar analysis can also be carried out for other possible bunching configurations involving multiple neighbouring fibrils. We find that the critical fibril length for multiple fibrils bunching is no less than that given by Eq. (3). It seems that the anti-bunching condition between two fibres is the most critical condition against bunching involving multiple fibres.

2.4. Fractal-like gecko hairs: bottom-up designed hierarchical fibrillar structures. Given that the work

of adhesion can be enhanced to a larger value by adopting a "hairy" structure [20,27,32,33], the critical length for flaw tolerant adhesion, according to Eq. (1), can also be extended to a larger scale. Meanwhile, the increase in work of adhesion with each added level of hierarchy should be limited by the maximum length of the fibres allowed by the anti-bunching condition. In other words, bunching between fibres provides an upper limit on how much the flaw tolerant length scale can be extended by one level of hierarchy. In order to achieve flaw tolerant adhesion at macroscopic length scales, multiple levels of hierarchy will be needed. To demonstrate the principle of flaw tolerance via structure hierarchy, we propose a "fractal gecko hairs" model [1], in which a hierarchical fibrillar structure is made from multiple levels of self-affine "brush" structures, as shown in Fig. 5. In this structure, the tips of fibres at each level of hierarchy are assumed to be coated with a "brush" structure consisting of smaller fibrils from one level below. The flaw tolerance and anti-bunching conditions are applied to all hierarchical levels from nanoscale and up to ensure robustness and stability at all levels. That is, the robustness principle of flaw tolerance and the stability principle of anti-bunching are used to determine geometry of fibre at different scales. The density of fibres at each level is determined such that the work of adhesion is maximized at each level. This procedure can be iterated from the lowest level structure and up until all the hierarchical levels are determined.

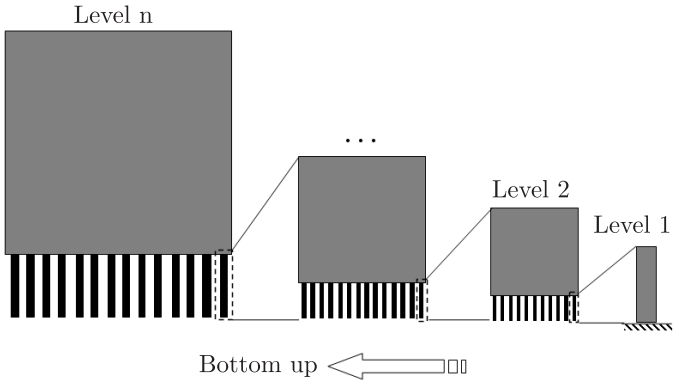

Fig. 5. Bottom-up design scheme of a hierarchical fibrillar structure. At each level, the fibres depend on smaller fibrils from the lower hierarchical levels as effective "adhesive bonds" with a surface. Interestingly, the fibres themselves act as "adhesive bonds" for larger fibres from higher hierarchical levels

Figure 6 shows the calculated hierarchical fibrillar structures following the bottom-up optimization procedure described above. In the calculations, we have taken the material properties of keratin as $E_f = 1.0$ GPa, $\nu_f = 0.3$, $\Delta\gamma = 10$ mJ/m^2, $\gamma_f = 5$ mJ/m^2 and $\sigma_{th} = 20$ MPa. Three lattice patterns, triangular, square and hexagonal, for the fibre array are considered. As shown in Fig. 6(a) and (b), both the fibre radius and length increase exponentially with the level of hierarchy. For the lowest level of structure, the critical fibre radius of flaw tolerant adhesion is only around 100 nm for the selected parameters . With hierarchical design, the flaw tolerant radius increases to 1 μm with 2 levels, 1 mm with 3 levels, 1 m with 4 levels of hierarchy. With 8 levels, the dimension of flaw tolerant radius has reached 10^{26} m, which is an astronomical size! These calculations demonstrate the enormous potential of a hierarchical structure for flaw tolerant adhesion. Fig. 6(c) displays the variation of the area fraction with the number of hierarchy levels. Interestingly, the area fraction converges to a constant after the third hierarchy level for each fibre layout pattern. Fig. 6(d) shows the work of adhesion at different hierarchical levels. In the first 6 levels, the triangular fibre pattern exhibits higher work of adhesion than the other two patterns. With further increase in hierarchy levels, this advantage is taken over by the hexagonal fibre pattern. Fig. 6(e) shows the effective adhesion strength which decreases and asymptotically approaches zero with increasing levels of hierarchy. However, the net pull-off force, as shown in Fig. 6(f), increases exponentially with increasing hierarchy. Fig. 6(g) illustrates the number N_n^f of fibrils on the tip of a fibre at the next level. We see that N_n^f increases sharply with increasing hierarchy levels.

2.5. Fibre fracture: an upper limit on flaw tolerant adhesion design. In the preceding discussions, we have focused our attention on failure along an adhesion interface and implicitly assumed that the fibres themselves do not fracture. In practice, as the adhesion strength is enhanced by introducing hierarchical fibrillar structures, the fracture of fibres eventually arises to become the dominant issue for failure at the system level.

Consider a single fibre at hierarchy level n. A penny-shaped crack is introduced in the center of the cross section as a possible internal flaw. Other configurations of crack-like flaws, such as edge/corner cracks/singularities, can be considered without affecting the basic idea. The critical tensile stress for fibre fracture can be determined from the Griffith's criterion for crack growth [38]. Considering a crack half the size of the fibre, this critical stress is

$$\sigma_n^{\max} = 1.63\sqrt{E_f^* \Gamma_f / R_n} \tag{4}$$

where Γ_f is the fracture energy of the fibre.

The relative significance of fibre fracture can be measured by a comparison between $\sigma_n^{\max}$ and the effective adhesion strength S_n at the n-th hierarchical level. If $\sigma_n^{\max} > S_n$, adhesion failure is regarded as the dominant issue and further increase in hierarchical levels can be considered. On the other hand, if $\sigma_n^{\max} < S_n$, fibre fracture is regarded as the dominant issue, hence an upper limit on the hierarchical design. Taking $\Gamma_f = 5$ J/m^2 and $E_f^* = 1$ GPa, we compare $\sigma_n^{\max}$ and S_n for the fractal hair structures constructed above. As shown in Fig. 7, for triangular and square fibre layout, only fibres within the first two levels satisfy the condition $\sigma_n^{\max} > S_n$; for the hexagonal layout, this condition is satisfied for the first three levels.

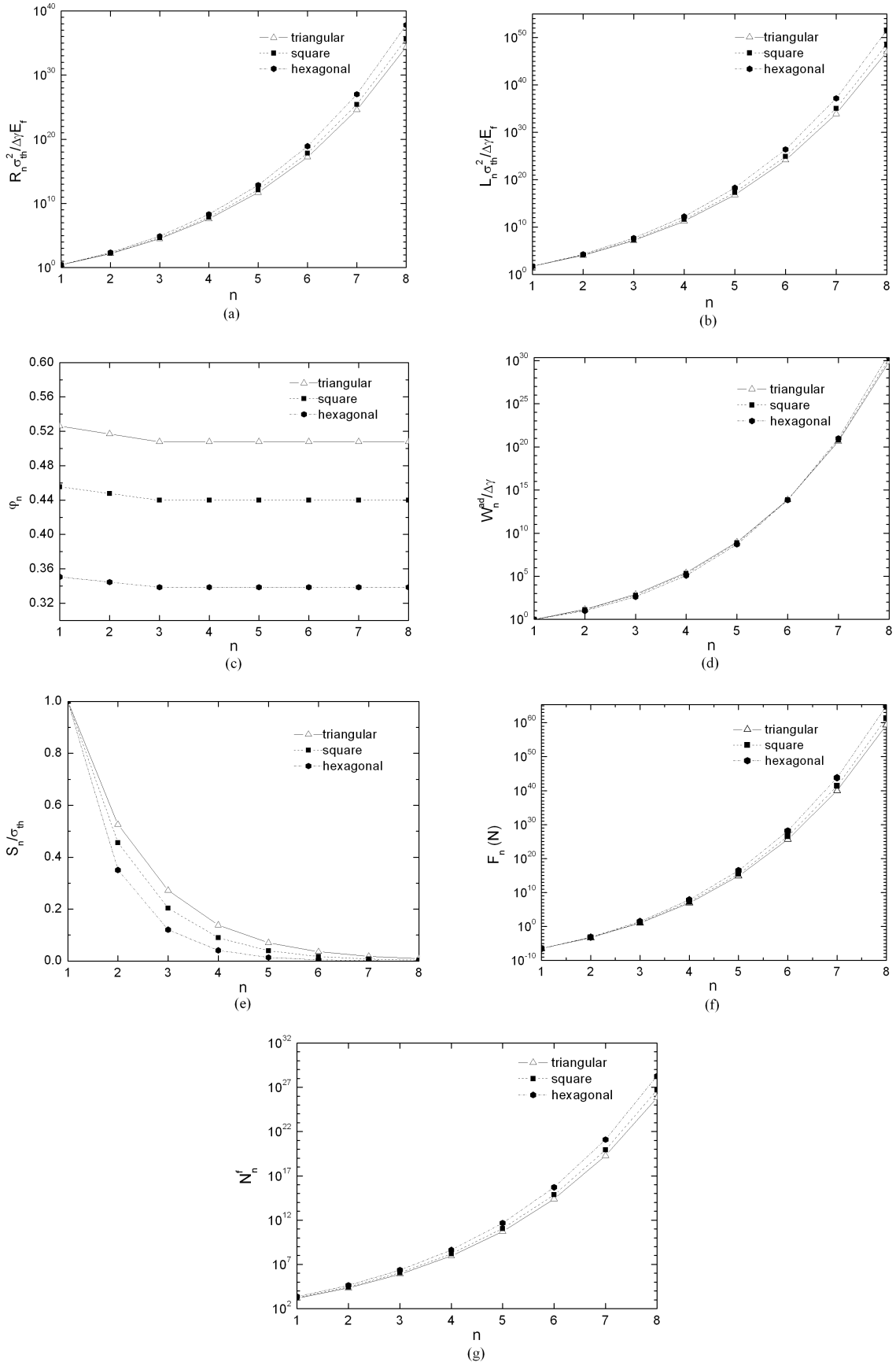

Fig. 6. Variations of (a) fibre radius R_n, (b) fibre length L_n, (c) area fraction φ_n, (d) work of adhesion W_n^{ad}, (e) adhesion strength S_n, (f) pull-off force F_n and (g) the number of fibres N_n^f as a function of the hierarchical level n

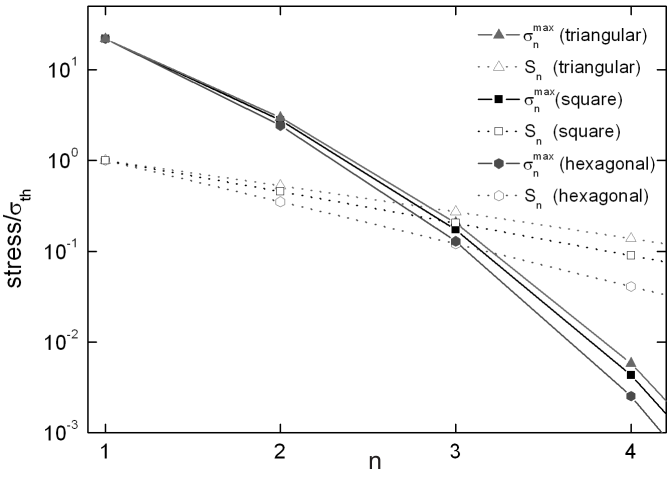

Fig. 7. Comparison between the fracture strength $\sigma_n^{\max}$ of a cracked fibre and the n-th level adhesion strength S_n of the bottom-up designed fractal hairs. If $\sigma_n^{\max} > S_n$, adhesion failure is regarded as the principal failure mode, otherwise ($\sigma_n^{\max} < S_n$) fibre fracture is thought of as the principal failure mode

Hence, although there is no upper bound for flaw tolerant adhesion via fractal hairs design, crack-like flaws in the hairs themselves would impose a practical limit for the usefulness of this strategy.

3. Releasable adhesion

For geckos and insects, robust adhesion alone is insufficient for survival as these animals need to move swiftly on walls and ceilings. The reversibility of attachment is just as important as the attachment. A conceivable strategy for reversible adhesion is to design an orientation-controlled switch between attachment and detachment, with adhesion strength varying strongly with the direction of pulling. An ideal scenario of robust and releasable adhesion is that the adhesion strength would be maintained near the theoretical adhesion strength when pulled in some range of directions, but then dramatically reduced when pulled in another range of directions. The switch between attachment and detachment thus can be accomplished simply by changing the pulling angles (e.g., by exerting different muscles). Some known examples of anisotropic adhesion systems in which the pull-off force varies strongly with the direction of pulling include an elastic tape on substrate [6,21,39] and a single seta of gecko sticking on a wall [3,24]. In the case of these single contact systems, the anisotropic behaviour of the pull-off force can be attributed to the asymmetric alignment and slender structure of the contacting object. While this behaviour suggests that the pull-off force of a single hair in contact with a substrate can be controlled by pulling in different directions, an open question is whether the adhesive strength of a large array of fibres or a macroscopic attachment pad in contact with a rough surface would show similar behaviours. To address this question, here we consider the issue of releasable adhesion from the viewpoint of continuum interfacial failure mechanics. We use theoretical modelling and numerical simulations to show that strong elastic anisotropy on the continuum level, achieved via fibrillar microstructures or some other means, plays a key role in releasable adhesion: a strongly anisotropic elastic solid also exhibits a strong orientational dependence of the pull-off force, similar to the behaviour of a single seta studied by Gao et al. [24].

3.1. Orientation-dependent adhesion strength of an anisotropic elastic material. To illustrate the intrinsic orientation-dependence of adhesion strength of an anisotropic elastic material in contact with a rough surface, we consider the linear elastic plane-strain problem shown in Fig. 8(a) where a transversely isotropic elastic half-space ($y \geqslant 0$) is brought into contact with a rigid substrate. A plane-strain interfacial crack of size $2a$ is used to represent random contact flaws due to surface roughness or contaminants. Although the actual adhesion strength depends on the crack size, the ratio between the maximum and minimum pull-off stresses as the pulling angle varies will be shown to be independent of the crack geometry and can be used as a measure of the releasability of adhesion.

In this interfacial crack model, the longitudinal direction of the material (y_0 axis) is tilted at an angle θ from the tangent of the substrate surface (x-axis). A remote uniaxial tensile stress σ^∞ is applied at an angle ϕ with respect to the x-axis. The transversely isotropic material is characterized by five independent elastic constants: E_t, E_l, ν_t, ν_l and μ. E_t and E_l stand for the transverse (x_0 direction) and longitudinal (y_0 direction) Young's moduli; ν_t, ν_l are Poisson's ratios associated with transverse (x_0 direction) and longitudinal (y_0 direction) loading; μ denotes the shear modulus in the $x_0 - y_0$ plane.

We are interested in the pull-off stress of the above adhesion system as a function of the pulling direction. This problem can be solved as a classical interfacial crack between two dissimilar anisotropic elastic solids [40–45]. For a remote tensile stress σ^∞ applied at an inclined angle ϕ, it can be shown that the pull-off stress is [1]

$$\sigma_{\rm cr}^{\infty}(\theta,\phi) = \frac{\sqrt{W_{ad}/\pi a}}{\sin\phi\sqrt{C[D_{22}\cos^2(\theta-\phi) + D_{11}\sin^2(\theta-\phi)]}}, \tag{5}$$

where C, D_{11}, D_{22} are constants dependent on the material elastic constants.

Given material constants and the anisotropy direction θ, Eq. (5) indicates that the adhesion strength varies as a function of the pulling angle ϕ. If the Young's modulus in the longitudinal direction (e.g., along a fibre array) is much greater than that in the transverse direction (e.g. transverse to the fibre direction), i.e. $E_l/E_t \gg 1$, according to Eq. (5), $\sigma_{\rm cr}^{\infty}(\theta,\phi)$ reaches its maximum and minimum when $\phi = \theta$ and $\phi = \theta/2 + \pi/2$ respectively. The adhesion releasability can thus be measured by the ratio of the maximum to the minimum pull-off stresses:

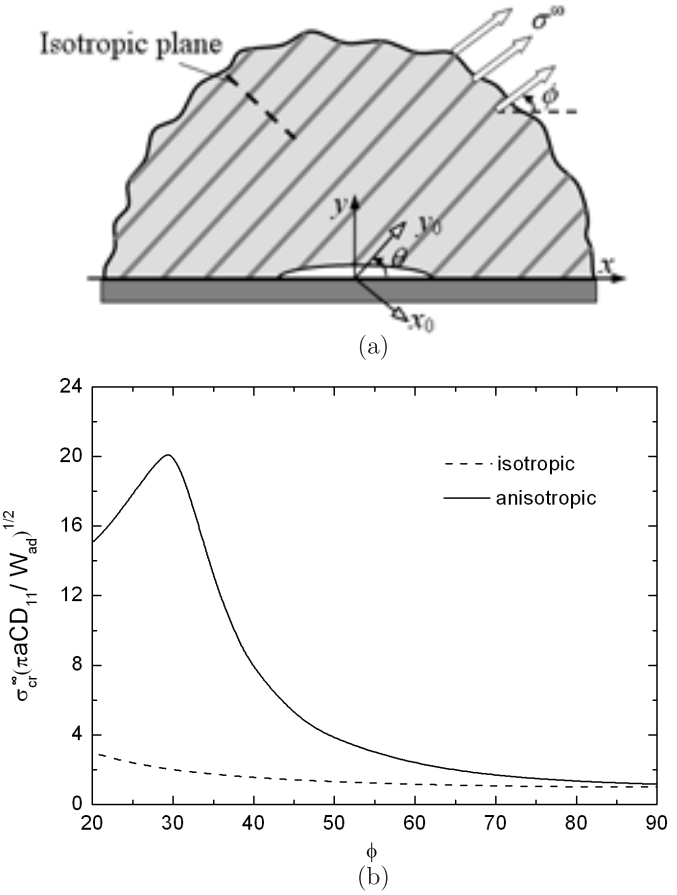

Fig. 8. The pull-off stress of a strongly anisotropic (transversely isotropic) elastic half-space sticking to a substrate. (a) An interfacial crack-like flaw with width $2a$ is introduced as a representative contact flaw due to surface roughness or contaminants. (b) Variation of the adhesion stress as a function of the pulling angle for the anisotropic material in comparison with that for an isotropic material

$$\frac{(\sigma_{\rm cr}^{\infty})_{\max}}{(\sigma_{\rm cr}^{\infty})_{\min}} = \frac{(1+\cos\theta)}{2\sin\theta}\left(\frac{D_{11}}{D_{22}}\right)^{1/2} = \frac{(1+\cos\theta)}{2\sin\theta}\left[\frac{E_l^2\left(1-\nu_t^2\right)}{E_t\left(E_l-\nu_l^2E_t\right)}\right]^{1/4}. \tag{6}$$

For small Poisson's ratios, Eq. (6) suggests that the releasibility of adhesion mainly depends on the stiffness ratio E_l/E_t and the anisotropy direction θ . The stronger the material anisotropy, the higher the adhesion releasibility. Assuming $\nu_t = \nu_l = 0.3$, $\theta = 30^\circ$ and $E_l/E_t = 10^4$, Fig. 8(b) plots the normalized pull-off stress as a function of the pulling angle ϕ. We can see that the elastic anisotropy causes about an order of magnitude change in adhesion strength as the pulling angle varies. A switch between attachment and detachment can be accomplished just by shifting the pulling angle between these two directions. In contrast, for an isotropic material with $E_l = E_t$ and $\nu_l = \nu_t$ the adhesion strength is much less sensitive to the pulling direction. Therefore, strong elastic anisotropy can result in an orientation-controlled switch between attachment and detachment.

3.2. Orientation-dependent adhesion strength of an attachment pad: numerical simulation. To further verify the principle of orientation-controlled adhesion switch via strong elastic anisotropy, we have also performed numerical simulations of the adhesion of a strongly anisotropic attachment pad (mimicking the hairy structured tissue on gecko's feet) via a general-purpose finite element code Tahoe[1] with specialized cohesive surface elements for modelling adhesive interactions between two surfaces. The constitutive relation for the cohesive surface elements is specified in terms of a relation between the traction and separation across the contact interface. Tahoe supports a number of traction-separation laws including the Tvergaard-Hutchinson law [46] and the Xu-Needleman law [47]. In present simulations, the Tvergaard-Hutchinson law is adopted.

The simulation system consists of a plane strain anisotropic (transversely isotropic) elastic pad adhering to a rigid substrate with a crack situated at the central region of the contact interface (representing an adhesion flaw due to surface roughness), as shown in Fig. 9(a). A displacement-controlled load is applied on the upper surface. At a given displacement, summation of all the nodal forces on the upper surface gives the pulling force F with components F_x, F_y. The pulling angle is then calculated via $\phi = \tan^{-1}(F_y/F_x)$. Periodic boundary conditions are applied on left and right sides. For comparison, both isotropic case and anisotropic case are considered. Typical material constants and adhesion parameters (see Table 2 in paper [1]) are selected to simulate the detachment process of the pad. Fig. 9(b) plots the normalized pull-off stress $F_{\rm c}(\phi)/(A\sigma_{\max})$ as a function of the pulling angle ϕ. In the anisotropic case, saturation of adhesion strength is observed in the vicinity of $\phi = \theta = 30^\circ$, corresponding to a plateau of the curve in the range of $20^\circ < \phi < 40^\circ$. If the pulling angle deviates from this range in either direction, the adhesion strength decreases quickly to a lower plateau. This two-plateau adhesion strength is ideal for rapid switch between attachment and detachment during animal movement. The ratio between the maximum and minimum strengths reaches four for the given geometry, giving rise to significant releasability. In contrast, for the isotropic cases, no variation in pull-off force is observed as the pulling angle varies. Therefore, we conclude that strong elastic anisotropy leads to releasable adhesion via an orientation-controlled switch between strong and weak adhesion.

4. Summary and discussion

We have studied the basic principles of robust and releasable adhesion in the hierarchical structures of gecko. The work has been inspired by comparative studies of

[1] http://tahoe.ca.sandia.gov

biological attachment systems in nature. For robust adhesion, we use a bottom-up designed fractal hair structure as a model to demonstrate that hierarchical fibrillar structures can lead to robust adhesion at macroscopic scales. Barring fibre fracture, we show that the fractal gecko hairs system can tolerate crack-like flaws without size limit. However, in practice, as the adhesion strength is enhanced by structural hierarchy, fibre fracture ultimately becomes the dominant failure mechanism and places an upper limit on the size scale of flaw tolerant adhesion. An optimal design is to introduce an appropriate number of hierarchical levels so that the adhesion interface and the hairs have similar strength levels. For releasable adhesion, we have shown that strong elastic anisotropy allows the adhesion strength to vary strongly with the direction of pulling. This orientation-dependent pull-off force enables robust attachment in the stiff direction of the material to be released by pulling in the soft direction. This strategy can be summarized as "stiff-adhere, soft-release".

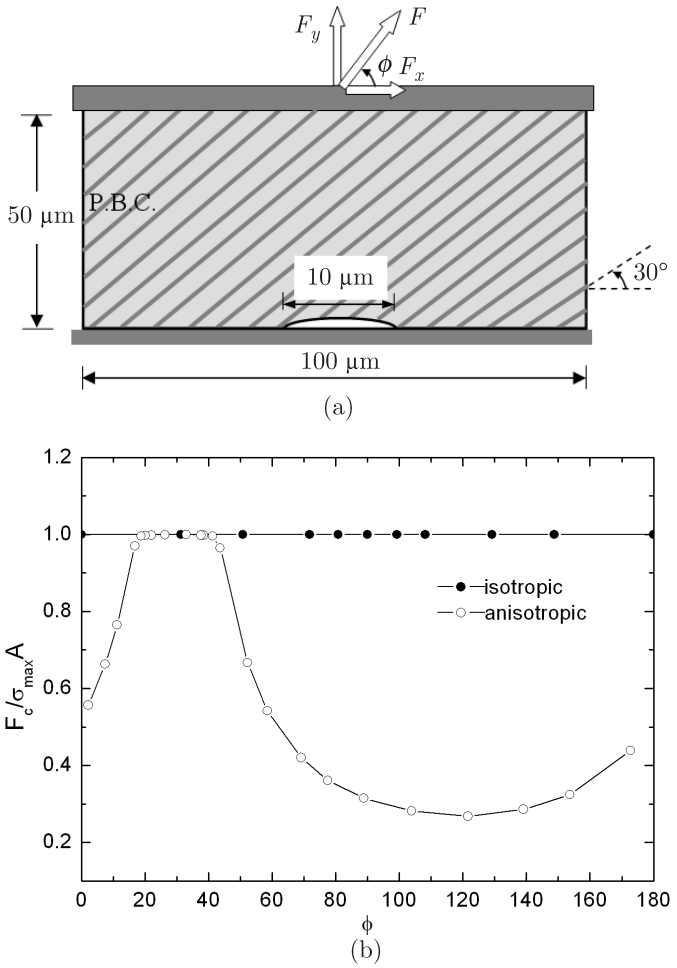

Fig. 9. Releasable adhesion in an attachment pad. (a) Geometry of the attachment pad used in FEM calculations. (b) Variation of normalized pull-off force with the pulling angle. P.B.C.: Periodic boundary condition

The complex hierarchical structures in biology provide a rich source of inspirations for physical sciences and industrial applications. The concepts developed in this paper should be of general value in understanding biological attachment devices and the design of synthetic adhesive systems in engineering [30,36]. Here we have considered the effects of hierarchical energy dissipation and elastic anisotropy on robust and releasable adhesion. Many other important aspects of the problem, such as viscoelasticity and large nonlinear deformation have not been taken into account. Much further work will be needed to advance our current understanding of bio-adhesion mechanisms. The studies on such problems should be of interest not only to the mechanics community but also to a variety of other disciplines including materials science, biology and nanotechnology.

Acknowledgements. This paper has been submitted to the Bulletin of the Polish Academy of Sciences: Technical Sciences on invitation by the editor. This paper is a modified version of an original paper [1] by the authors.

References

[1] H. Yao and H. Gao, "Mechanics of robust and releasable adhesion in biology: bottom-up designed hierarchical structures of gecko", *J. Mech. Phys. Solids* 54, 1120–1146 (2006).

[2] M. Scherge and S. Gorb, *Biological Micro- and Nanotribology*, Spinger-Verlag, New York, 2001.

[3] K. Autumn, Y.A. Liang, S.T. Hsieh, W. Zesch, W.P. Chan, T.W. Kenny, R. Fearing, and R.J. Full, "Adhesive force of a single gecko foot-hair", *Nature* 405, 681–685 (2000).

[4] K. Autumn, M. Sitti, Y.A. Liang, A.M. Peattie, W.R. Hansen, S. Sponberg, T.W. Kenny, R. Fearing, J.N. Israelachvili, and R.J. Full, "Evidence for van der Waals adhesion in gecko setae", *Proc. Natl. Acad. Sci.* 99, 12252–12256 (2002).

[5] K. Autumn and A.M. Peattie, "Mechanisms of adhesion in geckos", *Integr. Compar. Biol.* 42, 1081–1090 (2002).

[6] G. Huber, S. Gorb, R. Spolenak, and E. Arzt, "Resolving the nanoscale adhesion of individual gecko spatulae by atomic force microscopy", *Biol. Lett.* 1, 2–4 (2005).

[7] J.N. Israelachvili, *Intermolecular and Surface Forces*, 2nd ed., Academic Press, London, 1992.

[8] H. Hertz, "Über die Berührung fester elastischer Körper" ("On the contact of elastic solids"), *Reine Angew. Math.* 92, 156–171 (1882).

[9] K.L. Johnson, K. Kendall, and A.D. Roberts, "Surface energy and contact of elastic solids", *Proc. R. Soc. Lond.* A 324, 301–313 (1971).

[10] A.A. Griffith, "The phenomena of rupture and flow in solids", *Phil. Trans. Roy. Soc. Lond.* A 221, 163–198 (1921).

[11] B.V. Derjaguin, V.M. Muller, and Y.P. Toporov, "Effect of contact deformations on the adhesion of particles", *J. Colloid Interface Sci.* 53, 314–326 (1975).

[12] R.S. Bradley, "The cohesive force between solid surfaces and the surface energy of solids", *Phil. Mag.* 13, 853–862 (1932).

[13] D. Maugis, "Adhesion of spheres: the JKR-DMT transition using a Dugdale model", *J. Colloid Interface Sci.* 150, 243–269 (1992).

[14] D.S. Dugdale, "Yielding of steel sheets containing slits", *J. Mech. Phys. Solids* 8, 100–104 (1960).

[15] C.Y. Hui, J.M. Baney, and E.J. Kramer, "Contact mechanics and adhesion of viscoelastic spheres", *Langmuir* 14, 6570–6578 (1998).

[16] G. Haiat, M.C.P Huy, and E. Barthel, "The adhesive contact of viscoelastic spheres", *J. Mech. Phys. Solids* 51, 69–99 (2003).

[17] K.S. Kim, R.M. McMeeking, and K.L. Johnson, "Adhesion, slip, cohesive zones and energy fluxes for elastic spheres in contact", *J. Mech. Phys. Solids* 46, 243–266 (1998).

[18] E. Arzt, S. Enders, and S. Gorb, "Towards a micromechanical understanding of biological surface devices", *Z. Metallk.* 93, 345–351 (2002).

[19] E. Arzt, S. Gorb, and R. Spolenak, "From micro to nano contacts in biological attachment devices", *Proc. Natl. Acad. Sci.* 100, 10603–10606 (2003).

[20] B.N.J. Persson, "On the mechanism of adhesion in biological systems", *J. Chem. Phys.* 118, 7614–7621 (2003).

[21] R. Spolenak, S. Gorb, H. Gao, and E. Arzt, "Effects of contact shape on the scaling of biological attachments", *Proc. R. Soc.* A 461, 305–319 (2005).

[22] B.N.J. Persson, "Nanoadhesion", *Wear* 254, 832–834 (2003).

[23] H. Gao and H. Yao, "Shape insensitive optimal adhesion of nanoscale fibrillar structures", *Proc. Natl. Acad. Sci.* 101, 7851–7856 (2004).

[24] H. Gao, X. Wang, H. Yao, S. Gorb, and E. Arzt, "Mechanics of hierarchical adhesion structures of geckos", *Mechanics of Materials* 37, 275–285 (2005).

[25] N.J. Glassmaker, A. Jagota, and C.Y. Hui, "Adhesion enhancement in a biomimetic fibrillar interface", *Acta Biomater.* 1, 367–375 (2005).

[26] H. Gao, B. Ji, I.L. Jäger, E. Arzt, and P. Fratzl, "Materials become insensitive to flaws at nanoscale: lessons from nature", *Proc. Natl. Acad. Sci.* 100, 5597–5600 (2003).

[27] H. Gao, B. Ji, M.J. Buehler, and H. Yao, "Flaw tolerant bulk and surface nanostructures of biological systems", *Mech. Chem. Biosys.* 1, 37–52 (2004).

[28] H. Gao and S. Chen, "Flaw tolerance in a thin strip under tension", *J. App. Mech.* 72, 732–737 (2005).

[29] C.Y. Hui, N.J. Glassmaker, T. Tang, and A. Jagota, "Design of biomimetic fibrillar interface: 2. Mechanics of enhanced adhesion", *J. R. Soc. Interface* 1, 35–48 (2004).

[30] M.T. Northen and K.L. Turner, "A batch fabricated biomimetic dry adhesive", *Nanotech.* 16, 1159–1166 (2005).

[31] J.A. Greenwood, "Adhesion of elastic spheres", *Proc. R. Soc. Lond.* A 453, 1277–1297 (1997).

[32] A. Jagota and S.J. Bennison, "Mechanics of adhesion through a fibrillar microstructure", *Integr. Comp. Biol.* 42, 1140–1145 (2002).

[33] T. Tang, C.Y. Hui, and N.J. Glassmaker, "Can a fibrillar interface be stronger and tougher than a non-fibrillar one?", *J. R. Soc. Interface* 2, 505–516 (2005).

[34] M. Sitti and R.S. Fearing, "Synthetic gecko foot-hair micro/nano-structures as dry adhesives", *J. Adhesion Sci. Technol.* 17, 1055–1073 (2003).

[35] C.Y. Hui, A. Jagota, Y.Y. Lin, and E.J. Kramer, "Constraints on microcontact printing imposed by stamp deformation", *Langmuir* 18, 1394–1407 (2002).

[36] A.K. Geim, S.V. Dubonos, I.V. Grigorieva, K.S. Novoselov, A.A. Zhukov, and S.Y. Shapoval, "Microfabricated adhesive mimicking gecko foot-hair", *Nature Mater.* 2, 461–463 (2003).

[37] N.J. Glassmaker, A. Jagota, C.Y. Hui, and J. Kim, "Design of biomimetic fibrillar interfaces: 1. Making contact", *J. R. Soc. Lond. Interface* 1, 23–33 (2004).

[38] J. Tada, P.C. Paris, and G.R. Irwin, *The Stress Analysis of Cracks Handbook*, 3rd ed., ASME Press, New York, 2000.

[39] K. Kendall, "Thin-film peeling-elastic term", *J. Phys. D: Appl. Phys.* 8, 1449–1452 (1975).

[40] M. Gotoh, "Some problems of bonded anisotropic plates with cracks along the bond", *Int. J. Fract. Mech.* 3, 253–265 (1967).

[41] J.R. Willis, "Fracture mechanics of interfacial cracks", *J. Mech. Phys. Solids* 19, 353–368 (1971).

[42] T.C.T. Ting, "Explicit solution and invariance of the singularities at an interface crack in anisotropic composites", *Int. J. Solids Struct.* 22, 965–983 (1986).

[43] Z. Suo, "Singularities, interfaces and cracks in dissimilar anisotropic media", *Proc. R. Soc. Lond.* A 427, 331–358 (1990).

[44] H. Gao, M. Abbudi, and D.M. Barnett, "On interfacial crack-tip field in anisotropic elastic solids", *J. Mech. Phys. Solids* 40, 393–416 (1992).

[45] C. Hwu, "Fracture parameters for the orthotropic bimaterial interface cracks", *Engr. Fract. Mech.* 45, 89–97 (1993).

[46] V. Tvergaard and J.W. Hutchinson, "The relation between crack growth resistance and fracture process parameters in elastic-plastic solids", *J. Mech. Phys. Solids* 40, 1377–1397 (1992).

[47] X.P. Xu and A. Needleman, "Numerical simulations of fast crack growth in brittle solids", *J. Mech. Phys. Solids* 42, 1397–1434 (1994).